existence of as many as five or six members of the melanocortin receptor gene family (*18*). The isolation of the MSH-R, the ACTH-R, and perhaps additional melanocortin receptor genes should provide a more detailed understanding of the control of melanocyte and adrenal cortical function and help explain the actions and pharmacology of melanocortins in the brain and other tissues.

REFERENCES AND NOTES

1. E. Hanneman *et al.*, in *Peptide Hormones as Prohormones: Processing, Biological Activity, Pharmacology*, J. Martinez, Ed. (Horwood, Chichester, United Kingdom, 1989), pp. 53–82.
2. J. B. Tatro, *Brain Res.* **536**, 124 (1990).
3. D. DeWied and J. Jolles, *Physiol. Rev.* **62**, 977 (1982).
4. M. T. Murphy *et al.*, *Science* **221**, 192 (1983).
5. E. Ellerkmann, G. M. Nagy, L. S. Frawley, *Endocrinology* **130**, 133 (1992).
6. J. G. Cannon, J. B. Tatro, S. Reichlin, C. A. Dinarello, *J. Immunol.* **137**, 2232 (1986).
7. J. B. Tatro *et al.*, *Cancer Res.* **50**, 1237 (1990).
8. D. I. Buckley and J. Ramachandran, *Proc. Natl. Acad. Sci. U.S.A.* **78**, 7431 (1981).
9. D. G. Grahame-Smith *et al.*, *J. Biol. Chem.* **242**, 5535 (1967).
10. L. M. Mertz and K. J. Catt, *Proc. Natl. Acad. Sci. U.S.A.* **88**, 8525 (1991).
11. J. Pawelek, *J. Invest. Dermatol.* **66**, 210 (1976).
12. W. C. Probst, L. A. Snyder, D. I. Schuster, J. Brosius, S. C. Sealfon, *DNA Cell Biol.* **11**, 1 (1992).
13. R. K. Saiki *et al.*, *Science* **230**, 1350 (1985).
14. J. B. Tatro *et al.*, *J. Clin. Invest.* **85**, 1825 (1990).
15. J. M. Pawelek, *Yale J. Biol. Med.* **58**, 571 (1985).
16. T. K. Sawyer *et al.*, *Proc. Natl. Acad. Sci. U.S.A.* **77**, 5754 (1980). 4-Norleucine, 7-D-phenylalanine α-melanocyte–stimulating hormone (NDP-MSH) is an extremely potent synthetic α-MSH analog that is resistant to enzymatic degradation.
17. A. Slominski, R. Costantino, J. Wortsman, R. Paus, N. Ling, *Life Sci.* **50**, 1103 (1992).
18. K. G. Mountjoy and R. D. Cone, unpublished data.
19. C. Gerard *et al.*, *Nucleic Acids Res.* **18**, 7142 (1990); L. A. Matsuda *et al.*, *Nature* **346**, 561 (1990).
20. E. R. Spindel, E. Giladi, P. Brehm, R. H. Goodman, T. P. Segerson, *Mol. Endocrinol.* **4**, 1956 (1990).
21. B. K. Kobilka *et al.*, *Proc. Natl. Acad. Sci. U.S.A.* **84**, 46 (1987).
22. M. Masu *et al.*, *Nature* **349**, 760 (1991).
23. H. Y. Lin *et al.*, *Science* **254**, 1022 (1991); H. Jüppner *et al.*, *ibid.*, p. 1024.
24. M. L. Applebury and P. A. Hargrave, *Vision Res.* **26**, 1881 (1986).
25. R. A. F. Dixon *et al.*, *EMBO J.* **6**, 3269 (1987).
26. S. S. Karnik, T. P. Sakmar, H. B. Chen, H. G. Khorana, *Proc. Natl. Acad. Sci. U.S.A.* **85**, 8459 (1988).
27. M. Devereux, U. Haeberli, O. Smithies, *Nucleic Acids Res.* **12**, 387 (1984).
28. Y. Masu *et al.*, *Nature* **329**, 836 (1987).
29. C. Chen and H. Okayama, *Mol. Cell. Biol.* **7**, 2745 (1987).
30. A. G. Gilman, *Proc. Natl. Acad. Sci. U.S.A.* **67**, 305 (1970).
31. Sequences of the human MSH-R and ACTH-R were originally obtained by PCR with human melanoma cDNA as a template and degenerate oligonucleotides from transmembrane domains III and VI as primers [Q.-Y. Zhou *et al.*, *Nature* **347**, 76 (1990)]. The transmembrane domain III oligonucleotide was 5′-GAGTCGACCTGTG[CT]G[CT][CG]AT[CT][AG]CIIT[GT]GAC[AC]G[CG]TAC-3′, and the transmembrane domain VI oligonucleotide was 5′-CAGAATTCAG[AT]AGGGCAIC-CAGCAGAI[CG][AG][CT]GAA-3′. Brackets indicate variable nucleotide positions containing one of the species indicated; I represents positions containing an inoside nucleotide. We then labeled a 300-bp Eco RI–Sal I PCR fragment by random priming and used it to screen a Cloudman S91 melanoma line cDNA library constructed in the λZAP vector (Stratagene). Eight independent clones were isolated after hybridization at moderate stringency [40% formamide, 1 M NaCl, 50 mM tris (pH 7.5), sodium pyrophosphate (0.1%), SDS (0.2%), salmon sperm DNA (100 μg/ml), and ×10 Denhardt's] at 42°C for 18 hours. We determined that the clones were derived from the same gene by restriction mapping and partial sequencing. Clone A was sequenced with the dideoxy method [F. Sanger, S. Nicklen, A. R. Coulson, *Proc. Natl. Acad. Sci. U.S.A.* **74**, 5463 (1977)]. Gene sequences encoding the human MSH-R and ACTH-R were isolated from a human genomic DNA library in the EMBL3 vector by random primer labeling of both PCR fragments and hybridization at high stringency (50% formamide at 42°C).
32. J. E. Gerst, J. Sole, E. Hazum, Y. Salomon, *Endocrinology* **123**, 1792 (1988); F. Solca, W. Siegrist, R. Dorzdz, J. Girard, A. N. Eberle, *J. Biol. Chem.* **264**, 14277 (1989).
33. RNA was prepared from each of the tissues shown with the guanidinium thiocyanate procedure [J. M. Chirgwin, A. E. Przbyla, R. J. MacDonald, W. J. Rutter, *Biochemistry* **18**, 5924 (1979)]. Equivalent amounts of total RNA (20 μg) were analyzed by electrophoresis on a 2.2 M formaldehyde–1.2% agarose gel, transferred to a Nytran filter (Schleicher and Schuell, Keene, NH), and hybridized with fragments spanning transmembrane domains III to VI of the human MSH-R, the murine MSH-R, or the human ACTH-R under moderately stringent conditions [45% formamide, 1 M NaCl, 50 mM tris (pH 7.5), sodium pyrophosphate (0.1%), SDS (0.2%), 100 μg/ml salmon sperm DNA, and ×10 Denhardt's] at 42°C for 18 hours. Before rehybridization, the probe was removed by incubation of the filter in 50% formamide, 10 mM tris (pH 8), 1 mM EDTA, and 0.1% SDS at 68°C for 1 hour. Ethidium bromide staining of ribosomal RNAs confirmed that equivalent amounts of intact RNA were loaded in each lane.
34. Adrenal tissue from a 1-year-old rhesus macaque was fixed for 24 hours in formalin (10%) in phosphate-buffered saline (PBS) and then incubated for 24 hours in sucrose (30%) in PBS. Sections (20 μm) were prepared and hybridized with a 648-nucleotide ^{35}S-labeled RNA antisense probe complementary to the coding sequence spanning transmembrane domains I through VI of the human ACTH-R. Sections were hybridized in 65% formamide in 0.26 M NaCl, ×1.3 Denhardt's, 13 mM tris (pH 8), 1.3 mM EDTA, and dextran sulfate (13%) at 65°C for 18 hours.

35. We thank S. Reichlin and J. Tatro for human melanoma samples, C. Passavant for the human genomic DNA library, R. Halaban for primary murine and human melanocytes and helpful discussions, P. Stenzel for human adrenal samples, the Oregon Regional Primate Center, Beaverton, for rhesus macaque tissue samples, and J. Shiigi and J. Tasnady for technical assistance in the preparation of the manuscript. Supported by NIH grant R01 DK43859-02 (R.D.C.).

28 April 1992; accepted 1 July 1992

Target Enzyme Recognition by Calmodulin: 2.4 Å Structure of a Calmodulin-Peptide Complex

William E. Meador, Anthony R. Means, Florante A. Quiocho*

The crystal structure of calcium-bound calmodulin (Ca^{2+}-CaM) bound to a peptide analog of the CaM-binding region of chicken smooth muscle myosin light chain kinase has been determined and refined to a resolution of 2.4 angstroms (Å). The structure is compact and has the shape of an ellipsoid (axial ratio ~2:1). The bound CaM forms a tunnel diagonal to its long axis that engulfs the helical peptide, with the hydrophobic regions of CaM melded into a single area that closely covers the hydrophobic side of the peptide. There is a remarkably high pseudo-twofold symmetry between the closely associated domains. The central helix of the native CaM is unwound and expanded into a bend between residues 73 and 77. About 185 contacts (<4 Å) are formed between CaM and the peptide, with van der Waals contacts comprising ~80% of this total.

Calmodulin (CaM) is a 148–amino acid protein present in all eukaryotic cells that serves as the primary receptor for intracellular Ca^{2+} (*1*). The three-dimensional structure of native CaM with four bound Ca^{2+} showed a dumbbell-shaped molecule in which two structurally similar globular domains, each containing a pair of Ca^{2+}-binding sites, were separated by an eight-turn solvent-exposed central α helix (*2*). Whereas the presence of this central helix in solution has been questioned (*3*), several lines of evidence suggested that some amino acids within this region, as well as in both hydrophobic pockets formed within the globular domains, were critical for target interaction (*1*, *4*). Calmodulin activates more than 20 enzymes in eukaryotic cells, and the CaM-binding domain has been identified in several enzymes. In each case, the CaM-binding regions consist of 18 amino acids in linear sequence, and, whereas they show considerable sequence diversity, most are predicted to form amphipathic helices (*5*). Consequently, synthetic peptide analogs of CaM-binding regions have been used to study the interaction with CaM by a variety of biophysical and biochemical techniques.

One of the most intensely studied CaM-dependent enzymes is the smooth muscle form of myosin light chain kinase (smMLCK).

W. E. Meador and F. A. Quiocho, Howard Hughes Medical Institute and Department of Biochemistry, Baylor College of Medicine, Houston, TX 77030.
A. R. Means, Department of Pharmacology, Duke University Medical Center, Durham, NC 27710.

*To whom correspondence should be addressed.

The sequence of the CaM-binding region of smMLCK, spanning residues 796 to 815 as previously identified (6, 7), is shown below.

```
Ala Arg Arg Lys Trp Gln Lys
 1   2   3   4   5   6   7

Thr Gly His Ala Val Arg Ala
 8   9  10  11  12  13  14

Ile Gly Arg Leu Ser Ser
15  16  17  18  19  20
```

The affinity of this peptide for CaM is 1 nM, which is similar to the activation constant of smMLCK (8). In addition to its CaM-binding property, residues 796 through 815 serve as a pseudosubstrate to intrasterically inhibit kinase activity in the absence of Ca^{2+}-CaM (7, 9). The first 12 amino acids of the peptide seem to be more involved in autoinhibition, whereas the amino acids primarily involved in CaM binding have been suggested to be residues 5 and 9 to 18 (7, 9, 10).

We have crystallized CaM in the presence of the peptide (11) and determined the x-ray structure to 2.4 Å resolution. The phases were solved by multiple isomorphous replacement (MIR) combined with anomalous scattering (Table 1). The initial atomic structure, consisting of four molecules in the asymmetric unit, was obtained by fitting separate fragments of the NH_2-terminal and COOH-terminal domains (12) of the 1.7 Å refined structure of the native CaM (13) to a 3.5 Å MIR electron density map. The segment that connects the two domains was then fitted. Finally, the remaining long helical density between the two domains (determined to be the bound peptide) was fitted for each molecule. The structure was refined by using the suite of programs in X-PLOR (14) at 2.4 Å to an R factor of 0.22 (Table 1). The quality of the electron density calculated with $(2|F_o| - |F_c|)$ and α_c coefficients is shown in Fig. 1 (15).

The structure of the CaM-peptide complex shows the following prominent features (Fig. 2). It is compact and has the shape of an ellipsoid with overall dimensions of approximately 50 by 30 by 25 Å. The NH_2- and COOH-terminal domains of CaM are in close association with contacts mainly between the COOH-terminal ends of helices II of the N-domain and VI of the C-domain. The bound peptide is engulfed by both domains in a manner akin to an articulated jaw. The interaction between helices II and VI, mainly of hydrophobic nature, serves as a latch. All eight helices of CaM (I to IV in the N-domain and V to VIII in the C-domain) are in close proximity to and wrap around the peptide.

A surprising revelation is the remarkable high symmetry between the two domains of CaM about a pseudo-twofold axis along the axis of view and at the center of the structure shown in Fig. 2. This twofold axis relates all of the helices of each lobe (between helices I and V, II and VI, III and VII, and IV and VIII), the loops connecting the helices, the large shallow hydrophobic pocket in each lobe, and the two pairs of calciums located at both ends of the ellipsoid.

The bound peptide, which is α-helical from residues 4 to 18 (16), lies in the tunnel running diagonal to the long axis of the ellipsoidal CaM molecule. This alignment results in an optimal overlap between the peptide and CaM. The close association of the two lobes of CaM creates a hydrophobic patch or arc with a considerable area that encompasses the hydrophobic pocket on each lobe (Fig. 2A). This hydrophobic arc, with a slight left-handed twist, interfaces with the hydrophobic side of the helical peptide. Residues Trp^5 and Thr^8 of the peptide occupy the hydrophobic pocket of the C-domain, whereas Ala^{14}, Ile^{15}, and

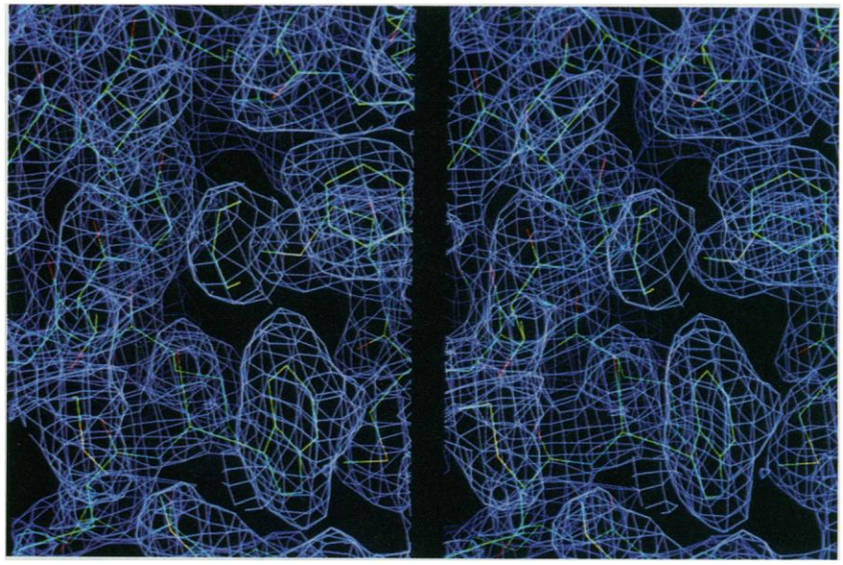

Fig. 1. Stereoscopic view of the 2.4 Å electron density of a portion of the peptide and its surrounding CaM residues superimposed with the refined structure. The electron density map (blue), calculated with coefficients $(2|F_o| - |F_c|)$ and α_c phases from the refined 2.4 Å resolution structure, was contoured at 1σ and grid spacings of 0.8 Å. Starting from the bottom of the figure, the peptide displayed is from residues Trp^5 to Val^{12}. The CHAIN program (29) was used for density fitting and molecular modeling.

Table 1. Crystallographic and refinement data. Abbreviations: U, uranyl acetate; Hg, potassium mercury tetraiodide; Sm, samarium acetate; Pb, lead nitrate; and RMS, root-mean-square. R_{merge} is the R factor on intensities for merging symmetry-related reflections; $R_{Cullis} = \Sigma||F_{PH} \pm F_P| - F_H|/\Sigma|F_{PH} - F_P|$; where F_{PH}, F_P, and F_H are the structure factors for the protein containing a heavy atom, the protein, and the heavy atom, respectively, and RMS $R_{anom} = |\Sigma(\Delta F_o^{\pm} - \Delta F_c^{\pm})^2/\Sigma(\Delta F_o^{\pm})^2]^{1/2}$, where $F_o^{\pm}$ and $F_c^{\pm}$ are the observed and calculated structure factors, respectively. The R factor is $\Sigma|F_o - F_c|/\Sigma|F_o|$.

Parameter	Native	U	Hg	Sm	Pb
Resolution limit (Å)	2.4	3.5	4.0	4.0	3.5
R_{merge}*	0.068	0.066	0.071	0.049	0.046
MIR statistics†					
Sites (no.)		7	12	8	12
f_H/residual		1.24	0.97	0.98	2.73
R_{Cullis}		0.90	0.88	0.89	0.52
RMS R_{anom}				0.74	0.65
Refinement statistics					
R factor	0.220				
CaM atoms (no.)	4488				
Peptide atoms (no.)	644				
Calcium atoms (no.)	16				
RMS deviation from ideal bond distance (Å)	0.016				
RMS deviation from ideal angle (degrees)	3.46				

*Completeness of data varies from 83 to 89%. †Cycles of heavy-atom refinement and phase determination were performed with the PROTEIN program package (28).

Leu[18] reside in the N-domain pocket. Completing the arc, Ala[11] and Val[12] reside in the domain-domain latch region.

The superpositioning of the N-domains of the structures of the native and the CaM-peptide complex (Fig. 3) shows a portion of the central helix transformed into an "expansion joint" in the complex structure. As superpositioning of identical domains of the bound and unbound forms of CaM shows only minor differences in the lobes, the large conformational change in CaM upon peptide binding is manifested almost completely by changes of the helix ϕ and ψ angles of residues 73 to 77 (*17*). To our knowledge, the "bend" of about 100° and "twist" of about 120° between the two lobes of CaM upon binding represent the largest ligand-induced interdomain motion in a protein.

There are about 185 contacts (<4 Å) between the peptide and CaM. Of these contacts, 15% are hydrogen bonds and 80% are van der Waals contacts. All seven basic residues of the peptide make salt bridges with CaM. Figure 4 schematically depicts the residues of CaM that make contacts with the residues in the α-helical segment (residues 4 to 18) of the peptide and also provides a description of the contacts associated with the first three and last two peptide residues. It is noteworthy that all nine Met residues of CaM, especially Met[72], are involved in interaction with the peptide.

The asymmetry of the structure, with the bend region proximal to the COOH-terminus of the peptide, reveals a further aspect of CaM binding. Since Arg[17] of the peptide is the only residue that extensively interacts by way of hydrogen-bonding and charge-coupling interactions with the bend and the helices preceeding and following the bend, (Figs. 2A and 4), it helps maintain the bent structure. This interaction provides a structural basis for the stringent requirement for an Arg at position 17 for CaM binding of several CaM-dependent enzymes (*1*) as well as for the observations that increasing or decreasing the length of the central helix by two to four residues has little effect on affinity for CaM (*18*).

The structure of the CaM-peptide complex differs markedly from proposed models (*19, 20*) of complexes of CaM with target proteins primarily because of differences in the arrangement of the two lobes and thus in the geometry of the bend or loop of the central helix and the mode of binding of the peptide segment. Moreover, Persechini and Kretsinger (*19*), modeling the CaM-binding segment of skeletal muscle MLCK, which is very similar to the smMLCK peptide shown above, positioned the peptide in the reverse direction to that seen in the structure. The orientation in the structure agrees with the nuclear magnetic resonance

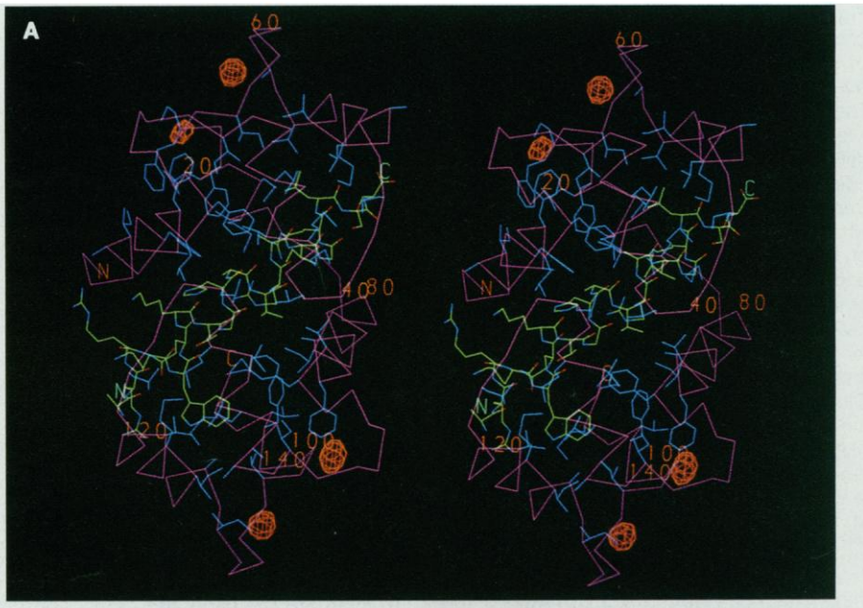

Fig. 2. Structure of CaM-peptide complex. (**A**) Stereoscopic view depicting the α-carbon backbone trace of CaM (magenta) and the complete structure of the bound peptide (color by atom types). Calciums are depicted as difference electron density surface (orange); the density (contoured at 5σ) was calculated with coefficients ($|F_o| - |F_c|$) and α_c phases from the 2.4 Å refined structure with the contribution of the calciums omitted. Every 20 residues of the α-carbon of CaM are identified. Hydrophobic side chains of CaM are shown (blue). (**B**) Perspective view of the α-carbon backbone traces of CaM (tan) and the peptide (green). Calciums are colored blue, and the helices identified by Roman numerals. This figure especially portrays the pseudo-twofold axis (perpendicular to the page and at the center of the CaM molecule) that relates the first four helices (I to IV) in the NH_2-terminal lobe to the corresponding helices (V to VIII) in the COOH-terminal lobe. Light blue peptide side chains are Trp[5], Arg[17], and Leu[18]. Drawn with the RIBBON program (*30*).

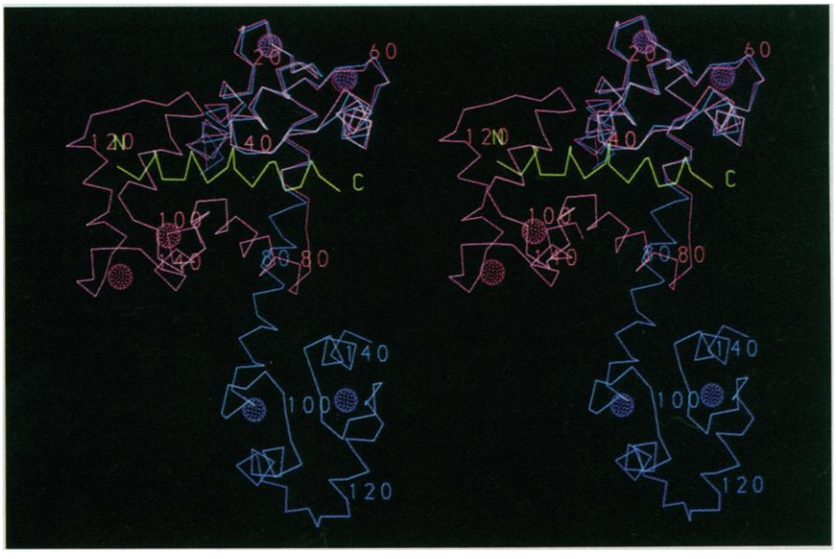

Fig. 3. Superposition of the structures of native CaM (blue) and CaM-peptide complex (magenta and green). See (*17*) for the ϕ and ψ torsion angles of the residues 73 to 77 in the bend region of the complex structure.

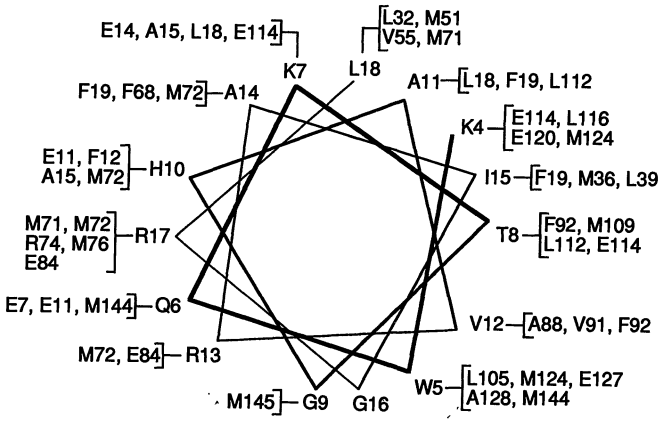

Fig. 4. Schematic diagram of the interactions (<4 Å distances) between CaM and peptide. The interactions are between the residues in the helical portion of the peptide (residues 4 to 18) (represented by a helical wheel) and the residues of CaM. The first three and the last two residues of the peptide form nonhelical turns. The α-ammonium group of Ala^1 salt links with Glu^{120}, Glu^{123}, and Glu^{127}, and the side chain contacts Met^{124}. Arg^2 salt links with Glu^{127} and contacts Met^{144}, and Arg^3 salt links with Glu^{14}. The last two residues (Ser^{19} and Ser^{20}) make very few contacts with CaM (at most three). Abbreviations for the amino acid residues are: A, Ala; C, Cys; D, Asp; E, Glu; F, Phe; G, Gly; H, His; I, Ile; K, Lys; L, Leu; M, Met; N, Asn; P, Pro; Q, Gln; R, Arg; S, Ser; T, Thr; V, Val; W, Trp; and Y, Tyr.

(NMR) data on smMLCK-CaM interaction (*21*). However, the pseudo-twofold symmetry of the two domains could in some cases allow binding in the reverse direction. The result of NMR studies of the mellitin-CaM complex is consistent with this possibility (*22*). Thus, the high symmetry between the two lobes could double the ways in which CaM could bind to target proteins. This, combined with the very large interaction surface of CaM, helps explain why CaM forms complexes with so many CaM-binding proteins that show little sequence identity. Despite divergent sequences, many synthetic peptide analogs of CaM-binding regions of CaM-dependent enzymes have similar high affinity for CaM (*23*). Even in the context of the MLCK enzymes, the CaM-binding regions can be exchanged between the skeletal and smooth muscle forms without affecting CaM activation properties (*24*). These diverse specificities are likely to be due to the predominant involvement of van der Waals contacts in target enzyme recognition and in the likely variability of the interdomain association.

The structure lends support to and new understanding of the results of extensive mutagenesis studies on interaction of CaM with smMLCK (*1*, *8*, *10*, *24*, *25*). For instance, it has revealed the molecular basis of the critical requirement of residues Trp^5, Arg^{17}, and Leu^{18} of the CaM-binding segment that are highly conserved in other target enzymes. Also of particular relevance is the observation that mutation of only three residues in the N-domain of CaM converts it from agonist to potent antagonist (*8*). The available data suggest that the N-domain of CaM might first interact with the COOH-terminal end of the smMLCK recognition sequence, which would allow the interaction of Arg^{17} with the CaM central helix and the Arg to act as a fulcrum to facilitate the bend and twist. The result would be a melding of the hydrophobic pockets in CaM to expose an array of apolar residues that would interact with the smMLCK peptide and pull it out of the active site of the enzyme in the activation process. Short-range electrostatic interactions between appropriate residues also contribute to the process. This proposal allows several predictions that can be tested by mutagenesis and structural analysis. Finally, the determination of the structure of the CaM-peptide complex herein described paves the way for the x-ray structure analysis of other CaM–target sequence complexes (*26*, *27*).

REFERENCES AND NOTES

1. A. R. Means, M. F. A. VanBerkum, I. C. Bagchi, K. P. Lu, C. D. Rasmussen, *Pharmac. Ther.* **50**, 255 (1991); C. B. Klee, and T. C. Vanaman, *Adv. Prot. Chem.* **35**, 213 (1982).
2. Y. S. Babu, C. E. Bugg, W. J. Cook, *J. Mol. Biol.* **204**, 191 (1988).
3. D. B. Heidorn and J. Trewhella, *Biochemistry* **27**, 909 (1988); K. Török, A. N. Lane, S. R. Martin, J.-M. Janot, P. M. Bayley, *ibid.* **31**, 3452 (1992); M. Kataoka, J. F. Head, T. Vorherr, J. Krebs, E. Carafoli, *ibid.* **30**, 6247 (1991).
4. M. Ikura, E. K. Lewis, M. Krinks, A. Bax, *ibid.*, p. 5498; S. M. Roth *et al.*, *ibid.* **31**, 1443 (1992).
5. L. G. McDowell, G. Sanya, F. G. Pendergast, *ibid.* **24**, 2979 (1985); J. A. Cox, M. Comte, J. E. Fitton, W. F. DeGrado, *J. Biol. Chem.* **260**, 2527 (1986); K. T. O'Neil and W. F. DeGrado, *Trends Biochem. Sci.* **15**, 59 (1990).
6. T. J. Lukas, W. H. Burgess, F. G. Pendergast, W. Lau, D. M. Watterson, *Biochemistry* **25**, 1458 (1986).
7. B. E. Kemp, R. B. Pearson, V. Guerriero, I. C. Bagchi, A. R. Means, *J. Biol. Chem.* **262**, 2542 (1987).
8. M. F. A. VanBerkum and A. R. Means, *ibid.* **266**, 21488 (1991).
9. R. B. Pearson, R. E. H. Wettenhall, A. R. Means, D. J. Hartshorne, B. E. Kemp, *Science* **241**, 970 (1988).
10. K. T. O'Neil, S. Erickson-Viitanen, W. F. DeGrado, *J. Biol. Chem.* **264**, 14571 (1989); I. C. Bagchi, Q. Huang, A. R. Means, *ibid.* **267**, 3024 (1992).
11. Crystals were obtained by the hanging-drop method. The drops consisted of 8 μl of CaM (24 mg/ml) and 4 μl of peptide (15 mg/ml) mixed with 12 μl of 25% w/v polyethylene glycol (PEG) 6000 (Fluka), 0.01% w/v sodium azide, 5 mM $CaCl_2$, and 50 mM Na acetate, pH 4.6. The wells contained 1 ml of 25% w/v PEG 6000 in the same buffer. The crystals belong to the space group $P2_12_12$ with unit cell dimensions a = 166.1 Å, b = 104.9 Å, and c = 44.3 Å and an asymmetric unit content of four molecules (a total of ~76 kD). Reliable native diffraction data from these crystals can be measured to 2.4 Å. All data sets were collected with a two-detector ADSC area detector system mounted on a Rigaku RU200 rotating anode x-ray generator (CuKα, 110 mA and 40 kV) with a graphite monochromator. Because the structure could not be determined by molecular replacement technique, it was solved by the MIR technique together with the anomalous scattering contribution. The 3.5 Å MIR phasing commenced with the location of the major K_2HgI_4 site in difference Patterson maps. Difference Fourier analysis yielded a total of 39 heavy-atom sites from the four derivatives used (Table 1).
12. For brevity, the NH_2-terminal and COOH-terminal domains or lobes of CaM are identified as N- and C-domains or lobes, respectively.
13. We have recently refined the 1.7 Å structure of the native CaM (R. Chattopadhyaya, W. E. Meador, A. R. Means, F. A. Quiocho, *J. Mol. Biol.*, in press).
14. A. T. Brünger, *X-PLOR Version 2.1: A System for Crystallography and NMR* (Yale University, New Haven, CT, 1990).
15. The detailed description of the structure determination and the structure will be published elsewhere; W. E. Meador, A. R. Means, F. A. Quiocho, in preparation.
16. In the four independent structures in the asymmetric unit, the four peptides are α-helical from Lys^4 to Leu^{18}. The first three and last two residues exist as coils.
17. The φ and ψ torsion angles (averaged over the four molecules in the asymmetric unit) of residues 73 to 77 in the bend region of the CaM-peptide structure are as follows: residue 73, φ = −93° ± 11.5° and ψ = −3° ± 3°; residue 74, φ = −59° ± 5° and ψ = 141° ± 7°; residue 75, φ = −89° ± 5° and ψ = 116° ± 7.5°; residue 76, φ = −92° ± 13° and ψ = 150° ± 13°; residue 77, φ = −74° ± 7° and ψ = 154° ± 7°.
18. J. A. Putkey, T. Ono, M. F. A. VanBerkum, A. R. Means, *J. Biol. Chem.* **263**, 11242 (1988); A. Persechini *et al.*, *ibid.* **264**, 8052 (1989); M. F. VanBerkum, S. E. George, A. R. Means, *ibid.* **265**, 3950 (1990).
19. A. Persechini and R. H. Kretsinger, *J. Cardiovasc. Pharmacol.* **12**, 501 (1988); *J. Biol. Chem.* **263**, 12175 (1988).
20. N. C. J. Strynadka and M. N. G. James, *Proteins* **7**, 234 (1990); T. Vorherr, O. Kessler, A. Mark, E. Carafoli, *Eur. J. Biochem.* **204**, 931 (1992).
21. S. M. Roth *et al.*, *Biochemistry* **31**, 1443 (1992).
22. S. H. Seeholzer *et al.*, in *Calcium-Binding Proteins in Health and Disease*, A. W. Norman, T. C Vanaman, A. R. Means, Eds. (Academic Press, New York, 1987), pp. 360–371.
23. D. K. Blumenthal *et al.*, *Proc. Natl. Acad. Sci. U.S.A.* **82**, 3187 (1985); R. M. Hanley *et al.*, *Science* **237**, 293 (1987); T. Vorherr *et al.*, *Biochemistry* **29**, (1990).
24. S. A. Leachman, P. J. Gallagher, B. P. Herring, M. J. McPhaul, J. T. Stull, *J. Biol. Chem.* **267**, 4930 (1992).
25. T. S. Lukas *et al.*, *Cold Spring Harbor Symp. Quant. Biol.* **63**, 185 (1988); M. O. Shoemaker *et al.*, *J. Cell Biol.* **11**, 1107 (1990); M. Ito, V. Guerriero, X. Chen, D. A. Hartshorne, *Biochemistry* **30**, 3498 (1991).
26. After submission of this report, an article appeared describing the solution NMR structure of Ca^{2+}-CaM complexed with a peptide analog of the skeletal muscle CaM–binding domain (*27*). The NMR structure and the x-ray structure reported here appear to be similar overall; however, the NMR structure shows the domain-domain interface distance to be slightly larger and the inter-

pretation of the pseudo-twofold symmetry to be different. With reference to Fig. 2 of this report and figure 3 in the article of Ikura *et al.* (*27*), helices II and VI are almost antiparallel in the crystal structure and at an angle in the NMR structure where the peptide Trp residue is also in a different conformation. The NMR structure describes a disordered region comprising residues 74 to 82. On the other hand, the crystal structure shows an extended peptide segment from residues 73 to 77, with well-defined helices preceeding (IV) and following (V) the segment. Thus we have obtained the ϕ and ψ torsion angles of the segment and have some understanding of the geometrical transformation in going to the CaM bound form from the unbound form. The origin of the differences between the NMR and x-ray structures is under investigation by both laboratories.

27. M. Ikura *et al.*, *Science* **256**, 632 (1992).
28. W. Steigemann, thesis, Technische Universität, München (1974).
29. J. S. Sack, *J. Mol. Graphics* **6**, 244 (1988).
30. M. Carson, *ibid.* **5**, 103 (1987).
31. We thank B. E. Kemp for the peptide sample and our colleagues in both laboratories for helpful discussions and assistance. Supported by the Howard Hughes Medical Institute and W. M. Keck Foundation (F.A.Q.), an NIH grant (A.R.M.), and a Cardiovascular Discovery Award from Glaxo (A.R.M. and F.A.Q.).

6 May 1992; accepted 24 June 1992

Deactivation of Visual Transduction Without Guanosine Triphosphate Hydrolysis by G Protein

Martha A. Erickson, Phyllis Robinson, John Lisman*

G proteins couple receptors to their target enzymes in many signal transduction cascades. It has generally been thought that deactivation of such cascades cannot occur without the hydrolysis of guanosine triphosphate (GTP) by G protein. This requirement has now been reexamined in both vertebrate and invertebrate phototransduction. Results indicate that GTP hydrolysis is not required for deactivation. Evidence is presented for an alternative model in which the target enzyme is deactivated by an inhibitory factor that is available even when GTP hydrolysis is blocked.

G protein–coupled receptors initiate signal transduction by catalyzing the exchange of GTP for guanosine diphosphate (GDP) on G proteins (*1*). The G protein with GTP bound to it can then activate its target enzyme. All steps in the cascade must deactivate when the signal is removed. According to what has become the standard model for G protein–mediated transduction, deactivation of the target enzyme depends directly on the hydrolysis of the bound GTP by the intrinsic GTPase of the G protein.

We questioned the standard model because it seems unable to account for the effect of nonhydrolyzable GTP analogs such as guanosine-5′-*O*-3-thiotriphosphate (GTPγS) (*2*) on G protein–mediated phototransduction in *Limulus*. If target enzyme deactivation cannot occur without GTP hydrolysis, each G protein that binds a nonhydrolyzable analog should generate a maintained increase in target enzyme activity and a maintained increase in the output of the transduction cascade. Thus, the G proteins that bind analogs during a stimulus should generate a maintained aftereffect, an output that persists even after the stimulus is removed (the response would normally return to base line). An aftereffect has been observed in *Limulus* photoreceptors (*3*, *4*) but surprisingly appears to be pulsatile waves (Fig. 1A, middle trace) rather than a maintained output. These spontaneous waves initiated at the G protein level are similar kinetically to the single photon response (*4*), the elementary unit of the light response, but have a smaller average size. We found no evidence of a concurrent maintained output because the average shift in resting potential was a negligible 0.46 ± 0.47 mV (SEM; $n = 4$). This complete return to base line after each wave indicates that the aftereffect is entirely pulsatile.

When further binding of GTPγS was induced by additional light, the pulsatile events became so frequent that they superposed to form a maintained, noisy aftereffect (Fig. 1A, bottom trace). The detection of the pulsatile nature of the aftereffect in *Limulus* photoreceptors is possible because the high transduction gain makes it possible to detect the events produced by a single G protein (*4*). In systems with less gain, only the larger maintained aftereffect resulting from the superposition of waves might be detected. Difficulty in explaining the pulsatile nature of the aftereffect in terms of the standard model led us to devise more rigorous tests of this theory.

According to the standard model, blocking hydrolysis should prevent any deactivation of the response at the offset of a long-duration light (*5*). Testing this prediction in living cells by injecting them with GTPγS is complicated by the fact that some deactivation will occur when G proteins bind endogenous, hydrolyzable GTP instead of the injected GTPγS. To estimate the relative binding of GTP and of the

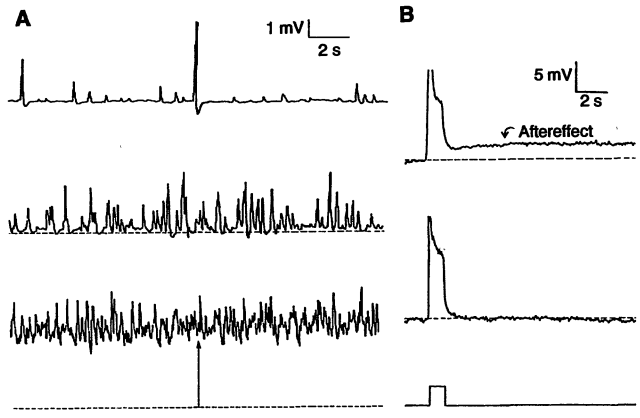

Fig. 1. Deactivation in *Limulus* ventral photoreceptors injected with GTPγS. (**A**) Pulsatile aftereffect of light in low intracellular concentration of GTPγS (≈20 μM). Top trace: before injection, low rate of spontaneous waves typical of these photoreceptors due to spontaneous activation of early stages of transduction (*23*). GTPγS was then pressure-injected, and light [50 flashes, 30-ms duration at 4×10^5 light-activated rhodopsin isomerizations (R*)/s] induced binding of GTPγS to G protein. The cell was then allowed to dark adapt. Middle trace: aftereffect of first light. The rate of waves in the dark was elevated but the base line was negligibly different from preinjection level (dashed line). Bottom trace: aftereffect of second identical light. Waves became so frequent that they superposed to form a maintained, noisy depolarization from the base line (arrow). Electrode contained 0.5 mM GTPγS, 10 mM Hepes, and 300 mM potassium aspartate, pH ≈ 7.0. (**B**) Deactivation of light response in high concentration of GTPγS. Top trace: receptor potential following injection of the GTPγS to 2.3 mM. At the termination of the long duration light (1 s, 5×10^5 R*/s) the voltage rapidly deactivated 80% from the plateau response, leaving only a small maintained aftereffect similar to that shown in Fig. 1A. For controls see (*24*). Middle trace: receptor potential following injection of GTP to 2.2 mM in a different cell. No aftereffect was elicited by light (1 s, 1×10^4 R*/s). Bottom trace: light stimulus. Electrode solutions: 100 mM GTPγS (or GTP, bottom trace), 4.5 mM Fast Green FCP, 300 mM potassium aspartate, 100 mM Hepes, and 5 mM KCl.

Biophysics Program, Department of Biochemistry, Department of Biology, and the Center for Complex Systems, Brandeis University, Waltham, MA 02254.

*To whom correspondence should be addressed.